Magnetic properties of ultrafine iron particles

S. Gangopadhyay and G. C. Hadjipanayis
Department of Physics and Astronomy, University of Delaware, Newark, Delaware 19716

B. Dale, C. M. Sorensen, and K. J. Klabunde*
Department of Physics, Kansas State University, Manhattan, Kansas 66506

V. Papaefthymiou and A. Kostikas†
Department of Physics, University of Ioannina, Greece
(Received 17 July 1991; revised manuscript received 16 December 1991)

The magnetic and morphological properties of fine Fe particles have been studied. Ultrafine particles of Fe were prepared using a vapor deposition technique under an argon atmosphere. The argon pressure was varied from 0.5 to 8 Torr during evaporation, and samples with a median diameter in the range 50–200 Å were obtained having a log-normal distribution. The dependence of magnetic properties on particle size and temperature ($10\ \mathrm{K} < T < 300\ \mathrm{K}$) were studied using superconducting-quantum-interference-device magnetometry and Mössbauer spectroscopy. Samples with particle diameter below 90 Å showed a superparamagnetic behavior below room temperature. The saturation magnetization of the particles varied from 25 to 190 emu/g, with the higher values corresponding to larger particles. For these larger particles, a coercivity of 1.05 kOe was obtained at room temperature. The magnetic and structural data suggested a core-shell type of structure, where the core consists of metallic Fe and the shell is composed of Fe oxides.

I. INTRODUCTION

Research on ultrafine particles (UFP's) has been fairly active in the last several years because of the wide range of potential applications, including magnetic recording media, ferrofluids, catalysts, medical diagnostics, drug-delivery systems, and pigments in paints and ceramics.[1,2]

UFP's can be made by various methods, with vapor deposition as one of the most widely used techniques. This technique has been used by several researchers[3–6] to obtain UFP's of magnetic materials such as Fe, Co, Ni, and their alloys. The particles produced by this method can exhibit a size ranging from 5 to 200 nm, which depends on the inert-gas environment, gas pressure during evaporation, and temperature of the source and substrate. It has been reported that a typical argon pressure of 3 Torr during evaporation yields a particle size of about 20 nm (Refs. 7 and 8) in fine particles of Fe and its alloys. The highest magnetization and coercivity reported for Fe particles was 160 emu/g and 1.1 kOe, respectively.[7] The difference in magnetization from the bulk value has been attributed to either the presence of nonmagnetic surface oxides or to the canting of moments in the oxide coating.[9–11] Earlier studies[12,13] have also shown the presence of surface layers of Fe oxides with a spinel structure, probably in the form of small crystallites. In fact in most studies an oxide layer was deliberately produced by controlled exposure to air in order to passivate the surface of the particles.

The present work explores in some detail the magnetic and structural properties of fine Fe particles prepared by evaporation in an argon atmosphere. In particular, the dependence of magnetic properties on particle size and temperature has been studied. Using the magnetic data we have estimated the thickness of the oxide shell, which surrounds the Fe core in a particle. Mössbauer spectroscopy has been used to study the surface oxides and the origin of high anisotropy in the Fe particles. Superparamagnetic samples have been obtained and their properties have been studied. Samples with saturation magnetization as high as 190 emu/g (made at 8 Torr argon pressure) and a corresponding room-temperature coercivity of 1.05 kOe have been obtained in this study.

II. EXPERIMENTAL METHOD

In the evaporation-deposition technique,[14–16] the metal to be deposited is vaporized in the presence of an inert gas. The metal vapors undergo collisions with the inert gas atoms resulting in nucleation of atoms to form particles. Then the growth process occurs which results in coagulation of the particles to form agglomerates. Gas pressure below 10 Torr can result in the formation of fine particles with sizes ranging up to a few hundred angstroms.

In the present work bulk Fe was evaporated from alumina-coated tungsten crucibles in an argon atmosphere at pressures in the range 0.5–8.0 Torr. During evaporation a thermal gradient was established between the source ($T \approx 1500\,^{\circ}\mathrm{C}$) and the copper substrate by keeping the substrate water cooled. This allowed collection of the particles on the copper substrate by thermophoresis. During evaporation a dynamic pressure of argon was maintained in the pressure range 0.5–8.0 Torr. A typical source-substrate separation of 2 cm was found

to give the maximum sample yield at a given argon pressure. An evaporation time of about 5–10 min was used to obtain sample masses varying from 5 to 10 mg. For Mössbauer studies, longer evaporation times of 30–45 min were used to obtain deposits up to 70 mg. A sample for electron microscopy was collected on a carbon coated Cu grid cemented to the water-cooled Cu substrate with diluted collodian. A separate shutter allowed a short time exposure (a few seconds) to collect a thin film of sample on the Cu grids. The temperature of the source during evaporation was determined using an optical pyrometer. Evaporation temperatures between 1260 and 1600 °C (±20 °C) were used for the different runs.

After evaporation, the specimens were subjected to a few hours soak in a dilute argon-air mixture (the volume ratio of argon to oxygen being about 3000) to passivate the surface as suggested by Tasaki.[7] The effect of different air volumes on the magnetic properties was studied in order to determine the optimum volume (the air volume resulting in the highest magnetization and coercivity values), which was used in the subsequent preparations. The specimens were then removed to the atmosphere, weighed, immobilized, and sealed from further contact with the atmosphere by mixing with molten wax in a quartz capsule. Mössbauer samples were prepared by sealing the powder in Perspex holders under inert N_2 atmosphere.

A superconducting-quantum-interference-device (SQUID) magnetometer was used to study the magnetic properties of the particles in the temperature range 10–300 K and in fields up to 55 kOe. Transmission electron microscopy and x-ray diffraction were used to study the particle shape, size, composition, and crystal structure.

Mössbauer data[17] were obtained with a constant acceleration spectrometer using a ^{57}Co(Rh) source at temperatures from 4.2 to 300 K. The data were used to determine the transition from ferromagnetic to superparamagnetic state and give information regarding the relative amounts of oxides and iron in the fine particles and the origin of high coercivity.

III. RESULTS AND DISCUSSION

A. Structure and particle morphology

X-ray diffraction and selected-area electron diffraction (SAD) showed mostly the presence of α-Fe, and a trace of either Fe_2O_3 or Fe_3O_4 (the peaks due to oxides were highly broadened indicating the presence of very small grains). Some samples had both oxides present and others had only one of them at a time. The metal-oxide mixture resulted because of the passivation process and the residual oxygen present in the chamber during evaporation. The diffraction rings due to α-Fe were much sharper in the case of samples with bigger diameter as compared to those with smaller diameter, as shown in Figs. 1(a) and 1(b) for samples with diameter of 200 and 68 Å, respectively.

Transmission electron microscopy (TEM) was used to study the crystal structure and particle morphology using both bright-field and dark-field electron micrographs. Nearly spherical particles with negligible shape anisotropy were obtained [Fig. 2(a)] in smaller particle samples. Tendency for forming chains among the particles was higher in samples with larger magnetization (as expected). Samples with smaller particles looked very fine in texture to the naked eye, whereas those with bigger particles formed needlelike agglomerate structures when scraped off the Cu substrate using a glass slide. TEM pictures [Fig. 2(b)] showed the presence of a darker particle center surrounded by a light colored coating in most of the particles. This could be attributed either to a core-shell type of structure, where the core consists of metallic α-Fe and the lighter shell due to its oxide, or due to other contrast effects in the microscope image such as those resulting from the thickness differences between the center and the edges of the particle due to its spherical shape. The results from dark-field TEM pictures showed a smaller median diameter as compared to their bright-field counterparts, which supports the former possibility of a core-shell type of structure.

About a hundred Fe samples were made and studied with their median diameter lying in the range 50–200 Å.

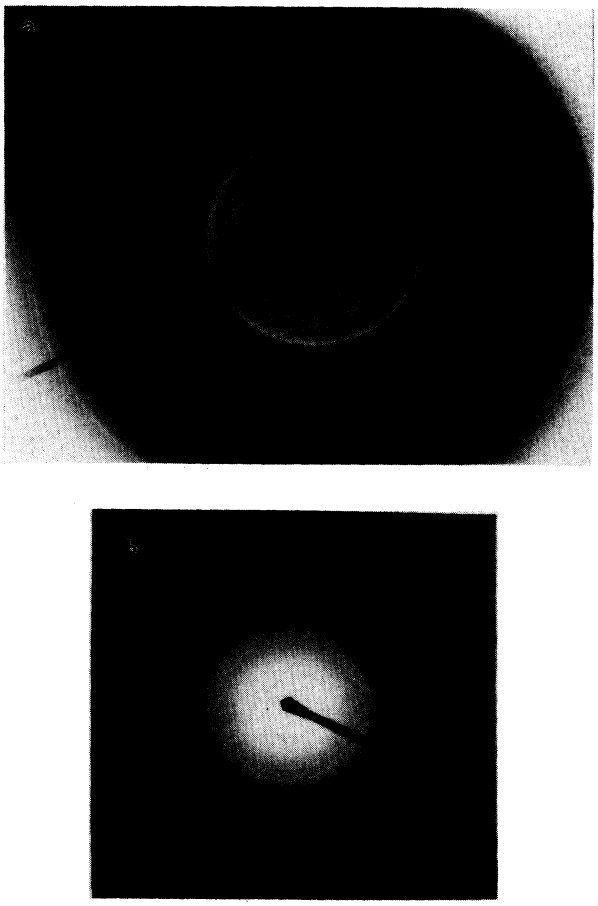

FIG. 1. (a) SAD of a sample with total diameter of 200 Å, showing sharp diffraction lines; (b) selected area diffraction pattern of a sample with total diameter of 68 Å, showing broad and diffuse lines.

The median diameter was determined by sampling different areas of the enlarged bright-field transmission electron micrograph. The particle size distribution obtained was found to resemble a log-normal distribution as shown in Fig. 3. It has been reported previously[5] that the geometric standard deviation for inert gas evaporated particles lies in the range $1.4 < \sigma < 1.6$. The Fe samples in our study have a value of σ between 1.1 and 1.3. The lower σ values being for smaller particles, indicating a tendency towards Gaussian distribution. Smaller size particles showed a narrower distribution compared to the bigger ones. A typical sample with a median diameter of 104 Å and a geometric standard deviation of 1.2 (which translates to an average standard deviation of 17 Å for a Gaussian distribution) is shown in Fig. 3. With increasing argon pressure from 0.5 to 8 Torr, a trend for increasing particle size was observed. This is due to the decrease in the mean free path of the Fe atoms as a result of the increase in the density of argon atoms inside the evaporation chamber (keeping other variables constant), leading to more collisions that form bigger particles. The particle sizes obtained in this study lie within the single domain particle regime for Fe (which is about 200 Å), and hence show some interesting properties.

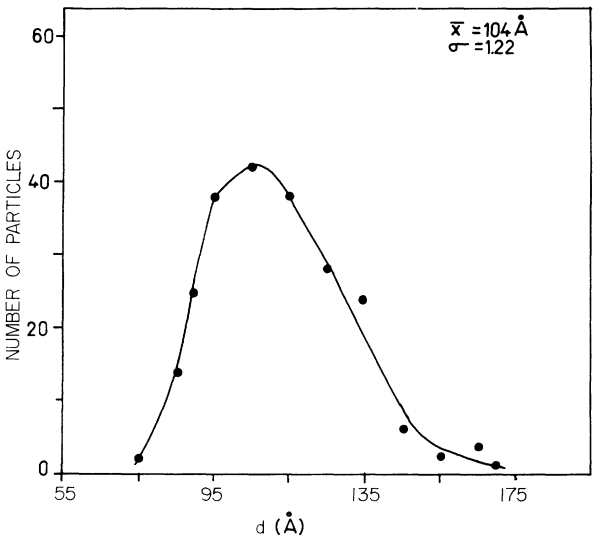

FIG. 3. Particle size distribution in a typical Fe sample showing log-normal distribution. It shows a median diameter of 104 Å and standard deviation of 1.22.

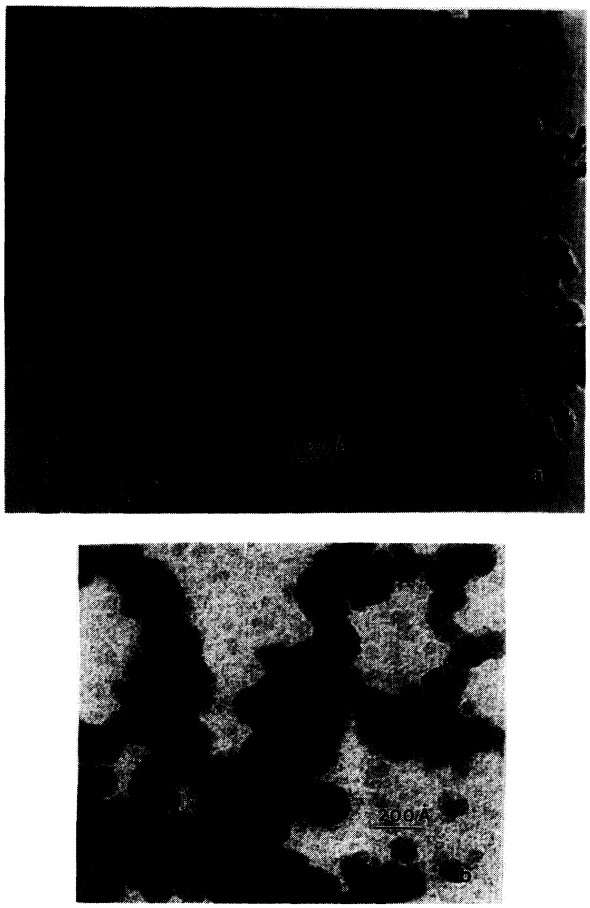

FIG. 2. (a) Bright-field micrograph showing nearly spherical particles of an Fe sample with median diameter of 110 Å; (b) bright-field TEM showing particles with clear dark centers surrounded by a light colored shell around them.

B. Magnetic properties

The magnetic properties of Fe particles depend strongly on particle size and the amount of oxidation. An extensive study has been made in order to understand the quantitative effect of these factors on the magnetic properties.

The saturation magnetization (M_S) was determined from M vs $1/H^2$ plots by extrapolating the value of magnetization to infinite fields. M_S was found to increase with increasing particle size. Magnetization values between 25 and 190 emu/g were obtained as the particle size was varied from 60 to approximately 200 Å, respectively (Fig. 4). A similar behavior for the magnetization was observed by Yamada *et al.*[18] in barium ferrite parti-

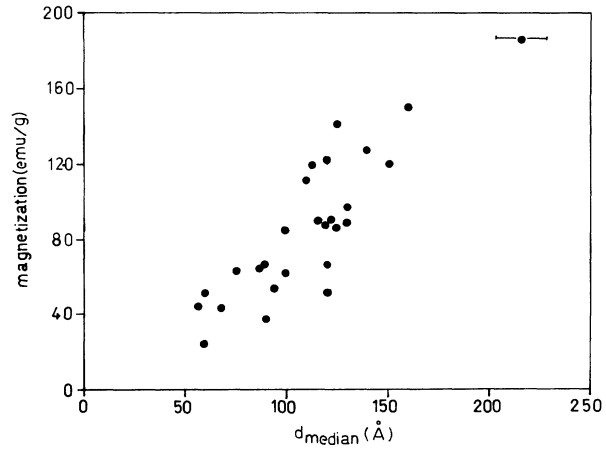

FIG. 4. Saturation magnetization vs median diameter, at 10 K. The maximum error in determining the median diameter is ±15 Å.

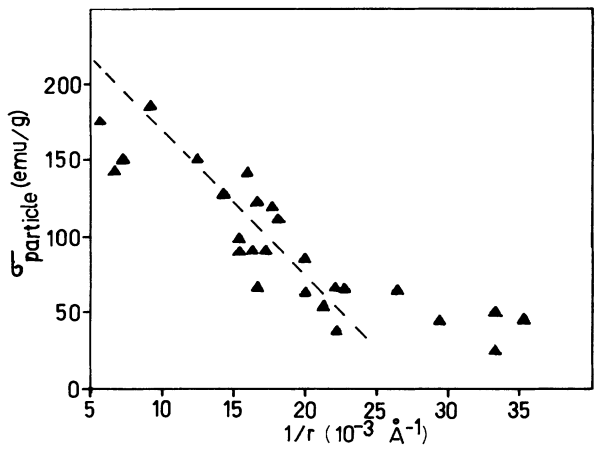

FIG. 5. Saturation magnetization as a function of the inverse of the total radius. The dashed line is the regression fit to the data, the slope is related to the shell thickness.

cles and by Kubo *et al.*[19] in $BaFe_{12-2x}Ti_xCo_xO_{19}$ fine particles. The decrease in magnetization with decreasing particle size is related to the higher surface to volume ratio in the smaller particles resulting in a much higher contribution from the surface oxide layer. The values of magnetization smaller than 80 emu/g (bulk saturation magnetization for Fe oxide) observed experimentally in smaller particles, may be due to the existence of nonmagnetic surface layers (dead layers[9,20]) around the particles or due to spin canting at the outer particle layers.[10,11,21]

If the magnetization is to vary with the surface area of the particle, the following expression [Eq. (2)] can be found from the linear weighted average of the magnetization [Eq. (1)] for a particle of total radius r, consisting of an Fe core surrounded by an oxide shell of thickness $dr \ll r$

$$\sigma_{particle} m_{particle} = \sigma_{core} m_{core} + \sigma_{ox} m_{ox} , \quad (1)$$

$$\sigma_{particle} = \sigma_{core} - 3[\sigma_{core} - \sigma_{ox}(\rho_{core}/\rho_{ox})](dr/r) , \quad (2)$$

where

$\sigma_{particle}$ = saturation magnetization of the sample in emu/g as determined from SQUID data ,

σ_{core} = saturation magnetization of the Fe core = 220 emu/g ,

σ_{ox} = magnetization for oxide layers in the range of 0–80 emu/g ,

$m_{particle}$ = mass of the particle = $m_{core} + m_{ox}$,

m_{core} = mass of the Fe core ,

m_{ox} = mass of the oxide shell of thickness dr ,

ρ_{core} = density of Fe core = 7.86 g/cm^3 ,

ρ_{ox} = density of oxide coating = 5.23 g/cm^3 (for Fe_3O_4) .

The magnetization does decrease linearly when plotted against the inverse of the radius except in samples with very small size where the assumption that $dr \ll r$ fails (Fig. 5). With a y intercept of 220 emu/g (for bulk Fe) the nonmagnetic oxide shell is established to be about 15 Å (Fig. 5). This linear dependence of magnetization on $1/r$ supports the proposition that the magnetization is indeed influenced by the surface of the particle.

A more rigorous analysis can be made without using the approximation used earlier ($dr \ll r$) to obtain a relationship between the core diameter and the total diameter of the particle (again taking a linear weighted average from an Fe core and an Fe-oxide shell around it):

$$d_{core} = \{(\rho_{ox}/\rho_{core})/[\rho_{ox}/\rho_{core} + (\sigma_{core} - \sigma_{particle})/(\sigma_{particle} - \sigma_{ox})]\}^{1/3} d_{total} , \quad (3)$$

where

d_{core} = core diameter, where the core is made of Fe ,

d_{total} = total diameter, including the core and the coating .

d_{core}, calculated from Eq. (3), was plotted against total diameter, d_{total} (Fig. 6), and assuming a nonmagnetic coating (or $\sigma_{ox} = 0$). From the linear regression fit to the data, the equation of the straight line was found to be

$$d_{core} = (0.85 d_{total} - 15) \text{ Å} . \quad (4)$$

From this the nonmagnetic shell thickness was found to increase from about 12 Å to 22 Å as the total particle diameter increased from 60 to 180 Å. This value is comparable to that obtained from the magnetization versus the inverse particle radius graph (Fig. 5). Similar numerical results on the oxide coating have been reported by other authors.[5,22,23] Tamura and Hayashi[22] calculated

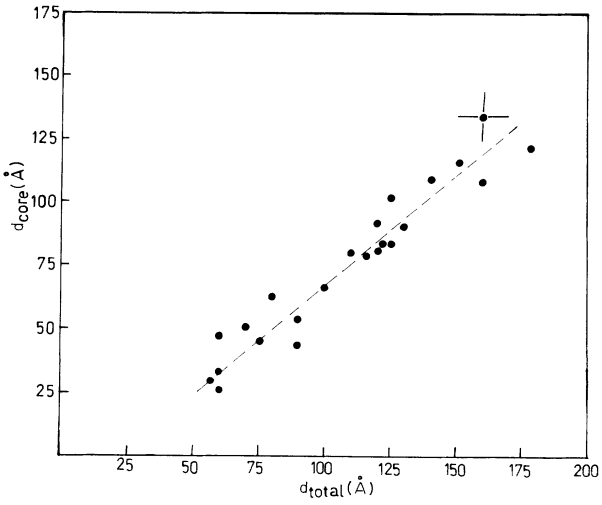

FIG. 6. Total median diameter vs the core diameter calculated using Eq. (2). The intercept of regression fit on the y axis is 15 Å, when extrapolated.

TABLE I. Atomic fraction of Fe atoms in the oxide and α-Fe phases and magnetization, for various particle sizes.

Particle size (Å)	wt. % of Fe	wt. % of Fe oxides	Magnetization (Mössbauer) (emu/g)	Magnetization (SQUID) (emu/g)	% error
275	41.6	58.4	144.6	150	3.6
214	27.8	72.2	126.6	135	6.22
113	30	70	129.5	120	−7.92
100	16.5	83.5	112	91	−23.08
88	7.3	92.7	100.2	65	−54.15

the oxide shell thickness in Fe particles made by gas evaporation method, to be about 12 Å using Mössbauer spectroscopy. Shinjo *et al.*[23] estimated the oxide shell thickness to be about 13 Å. This value was obtained by sputtering the surface of oxide-coated Fe particle using argon molecules in electron spectroscopy for chemical analysis (ESCA) measurements. Also a constant oxide thickness of 10 Å was observed by Granqvist and Buhrman[5] in fine Al particles made by gas evaporation.

The ability of Mössbauer spectroscopy to probe the magnetic state of Fe and its oxides was utilized in the temperature range 10–300 K. Typical Mössbauer spectra of a sample of particles with core diameter of 96 Å are shown in Fig. 7. The low-temperature spectra were analyzed with superposition of a magnetic hyperfine pattern due to α-Fe and an oxide component which, from the hyperfine parameters can be attributed to Fe_3O_4 or γ-Fe_2O_3.[17] Assuming equal Debye-Waller factors, the relative areas of the two components gave the atomic fraction of Fe atoms in the oxide and α-Fe phases (Table I).

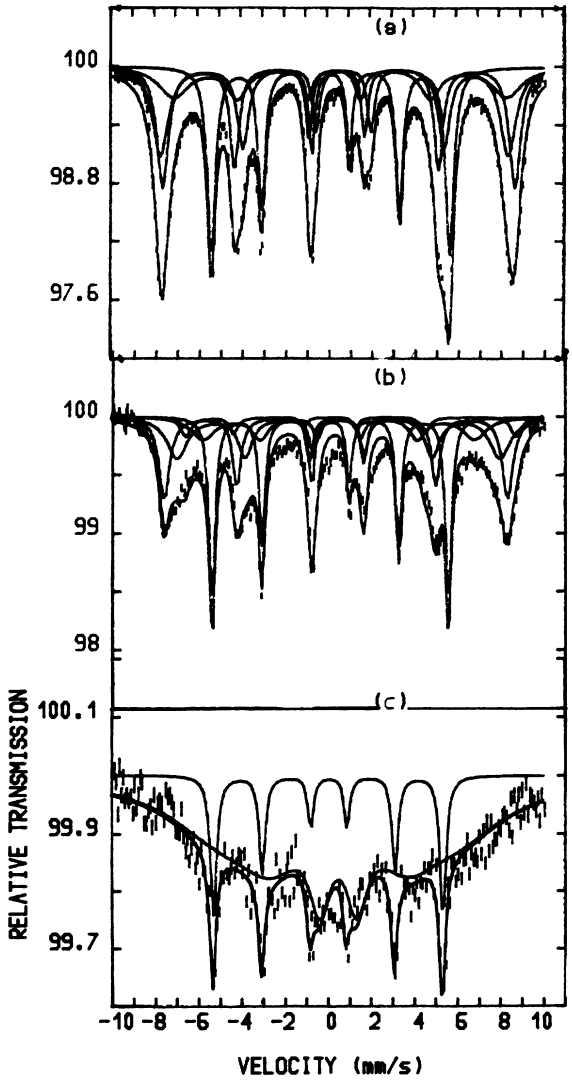

FIG. 7. Mössbauer spectra of an Fe sample with core diameter of 96 Å at three different temperatures: (a) 4.2 K (b) 85 K (c) 300 K.

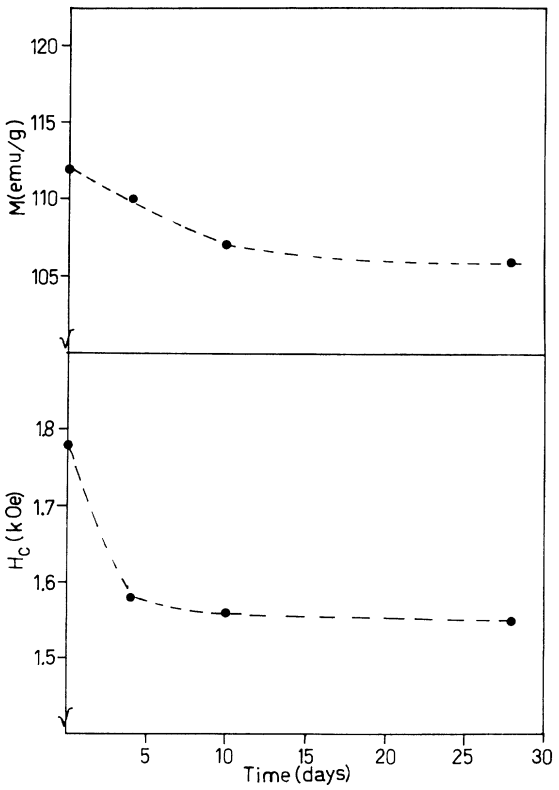

FIG. 8. Variation of magnetization and coercivity with time at $T=10$ K, for an Fe sample with core diameter of 130 Å.

Using these fractions and the values of saturation magnetization for α-Fe and γ-Fe_2O_3/Fe_3O_4 a predicted magnetization was found and compared to the experimentally measured value (Table I). For the larger particles the predicted and experimental magnetization values are in close agreement (within experimental error). For the smaller particles, however, where the percentage of Fe oxides is much larger, large deviations have been observed. These deviations can be explained by the spin canting proposed for ultrafine particles.[10,11,21]

Magnetic measurements were repeated on some of the samples in order to examine any aging effects. The samples packed in wax showed higher resistance to oxidation than those left in open air after preparation. The aging effect on the magnetic properties of samples with smaller size was more pronounced than in the bigger ones. Magnetization decreased by 25%, 3.8%, and 1.8% in samples with median core diameters of 25, 108, and 150 Å, respectively, over a time period of five days. The decrease in magnetization was larger at 10 K than at 300 K. The relative decrease in magnetic properties was much smaller as the sample aged more as shown in Fig. 8. The aging effect on coercivity was not drastically different in samples with different particle size as the magnetization was, but it also showed a similar trend.

C. Temperature dependence of magnetization

The temperature dependence of magnetization fits Bloch's[24] $T^{3/2}$ law as shown in Fig. 9. This is not very surprising because Fe has a high $T_c = 780\,^{\circ}C$; and since we are concerned with temperatures less than 27 °C, the spin-wave theory holds quite well in this temperature regime. According to this law,

$$M = M_s(1 - BT^{3/2}) \quad (\text{for } T \ll T_c)\,, \tag{5}$$

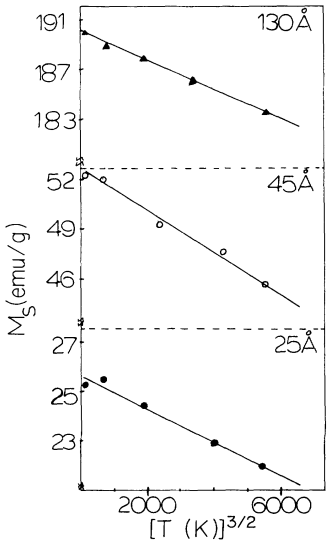

FIG. 9. Fitting the temperature dependence of saturation magnetization data to Bloch's $T^{3/2}$ law for spin waves, for samples with median core diameter of 130, 45, and 25 Å.

TABLE II. The temperature coefficient B [$\equiv A(k_B/J_l)^{3/2}$] for the magnetization M for some samples.

Particle size d_{core} (Å)	Magnetization (emu/g)	B ($K^{2/3}$)
130	190	6.0×10^{-6}
>100	123	5.5×10^{-6}
44	37	3.3×10^{-5}
33	52	2.5×10^{-5}
25	25	2.4×10^{-5}

where M_s is the saturation magnetization. $B = A(k_B/J_e)^{3/2}$ where $A = 0.1174$ for a simple-cubic lattice, k_B is Boltzmann's constant, and J_e the exchange constant.

The value of Bloch's constant for bulk Fe is 3.3×10^{-6} $K^{-3/2}$. Table II shows the value of "B" for some of the samples. For the smaller particles, B is found to be larger by an order of magnitude. From the above equation, this implies a stronger dependence of magnetization on temperature. A similar behavior was observed in granular Fe:SiO_2 solids.[25] Theories[26] have shown that the fluctuation of surface moments are larger than those of the interior so that B of the surface atoms is about 2–3.5 times larger than that of the interior. This explains the larger values of B in smaller particles, because the fraction of atoms present on the surface is much higher in the case of smaller particles, compared to the bigger ones. The problem, however, might be more complicated because of the possible lattice softening of the small particles[27] (and therefore softening of the spin waves) and the geometrical size effect limiting the value of the spin wavelength.[25]

D. Superparamagnetic fractions

As the volume of a ferromagnetic particle is reduced, a size is reached below which the anisotropy energy is smaller than the thermal energy. In that case, thermal fluctuations cause the magnetic moment of the domains to fluctuate randomly between their energy minima; hence the particles behave like a paramagnet. The superparamagnetic relaxation time τ at a temperature T is given by[28]

$$\tau = \tau_0 e^{KV/k_B T}\,,$$

where τ_0 is of the order of 10^{-10} s, K is the anisotropy constant, V is the volume of the particle, and k_B is Boltzmann's constant.

The temperature above which a superparamagnetic behavior is observed is referred to as the blocking temperature (T_B). Because of the differences in the measurement

TABLE III. Blocking temperature T_B for some samples.

Particle diameter d_{core} (Å)	T_B (K)
53	230
33	170
35	150
25	120

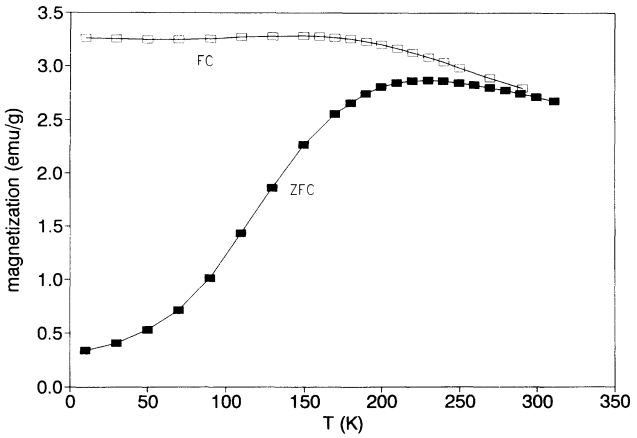

FIG. 10. Appearance of a peak near the blocking temperature due to superparamagnetism in a sample with core diameter of 53 Å. The sample was cooled in a zero field and the magnetization was then measured as a function of temperature, in an applied field of 50 Oe.

time (few seconds for SQUID magnetometer and 10^{-8} s for Mössbauer) the blocking temperatures determined by these two techniques are quite different, with the SQUID data showing a lower T_B. Fe particles with core diameter below 60 Å showed superparamagnetism when characterized with SQUID. The blocking temperature T_B for four samples is listed in Table III. T_B decreases with the decrease in particle size. The blocking temperatures listed are the average of the T_B's within a sample because of a finite-size distribution in the particle size. Above T_B, no remanence and coercivity were observed. The blocking temperature of superparamagnetic samples was also confirmed by a broad peak in the zero-field-cooled (ZFC) thermomagnetic data, shown in Fig. 10. The magnetic curves at different temperatures above the blocking temperature can be superimposed when plotted against H/T as shown in Fig. 11 for a sample with a median core diameter of 25 Å.

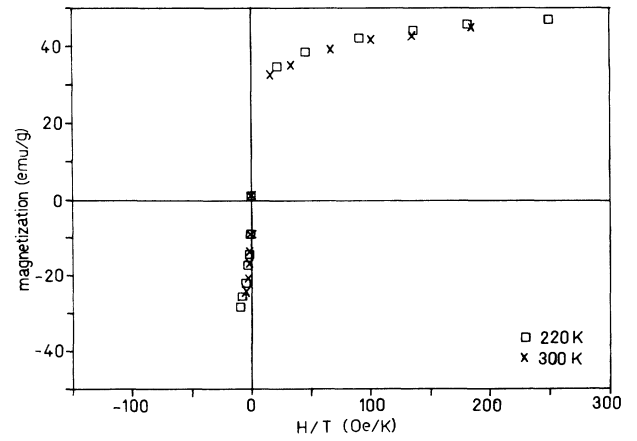

FIG. 11. Magnetization vs H/T for a superparamagnetic sample with core diameter of 33 Å. The magnetization curves are superimposed at two temperatures above T_B of the sample.

The superparamagnetic behavior of the particles was also made evident from their Mössbauer spectra. The room-temperature spectra [Fig. 7(c)] of all the samples were characterized by a broad absorption band superimposed on the sextet due to ferromagnetic α-Fe. Such behavior has also been observed by other authors.[12,22,23,29] Haneda and Morrish[12] attribute the broadness of the oxide spectrum at $T=300$ K, to the interaction between the superparamagnetic surface layer (consisting of small crystallites of Fe oxide) with the metallic Fe core. Tamura and Hayashi[22] explained this behavior by the asymmetry of the anisotropy fields present in the oxide surface layer consisting of a mixture of fine crystallites of Fe_3O_4 and γ-Fe_2O_3. A model proposed by Mørup and Topsøe[29] could also explain the oxide spectra at 300 K, by taking into account only the interaction among the oxide crystallites and ignoring the interaction with the Fe core (as long as the exchange interaction among the oxide crystallites dominates all other anisotropies in the system). In this study the structural results in conjunction with the strong temperature dependence of coercivity (explained in the next section) suggest a strong exchange interaction between the Fe core and the oxide shell, which could then explain the presence of the broad absorption band observed at $T=300$ K [Fig. 7(c)] due to the superparamagnetic Fe oxide.[12]

E. Coercivity

The coercivity (H_c) of the powders was found to depend strongly on particle size (Fig. 12). The decrease in H_c with decreasing particle size[30] is due to thermal effects observed in particles with a size below the single domain particle (the SDP size for Fe is $\approx$200 Å). At 10 K thermal effects are negligible and a different size dependence was observed as shown in Fig. 13. H_c decreased from a value of 3400 Oe to about 1500 Oe, as the particle's core diameter increased from 25 to 100 Å. Figure 13 also shows that for bigger particles the value of H_c at 10 K was independent of particle size, but it increased sharply as the particle size was decreased below 80 Å.

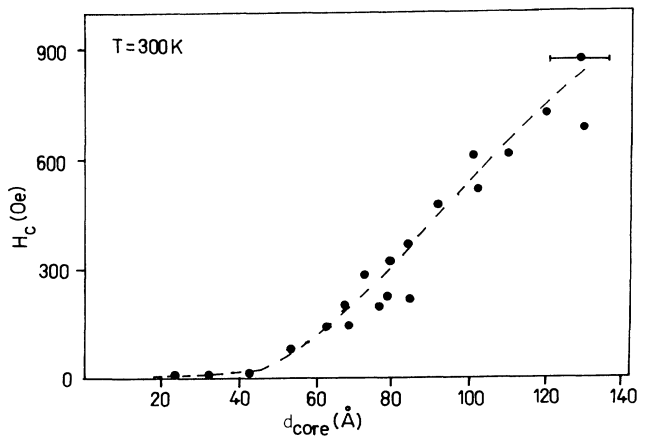

FIG. 12. Coercivity vs median core diameter at $T=300$ K; the dashed line is drawn to guide the eye.

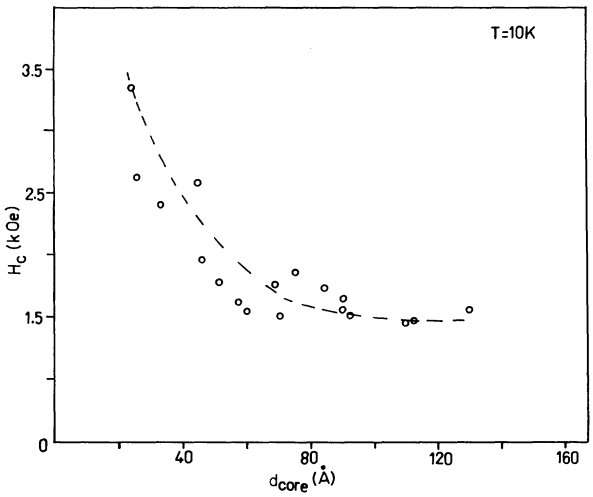

FIG. 13. Coercivity vs median core diameter at $T=10$ K; the dashed line is drawn to guide the eye.

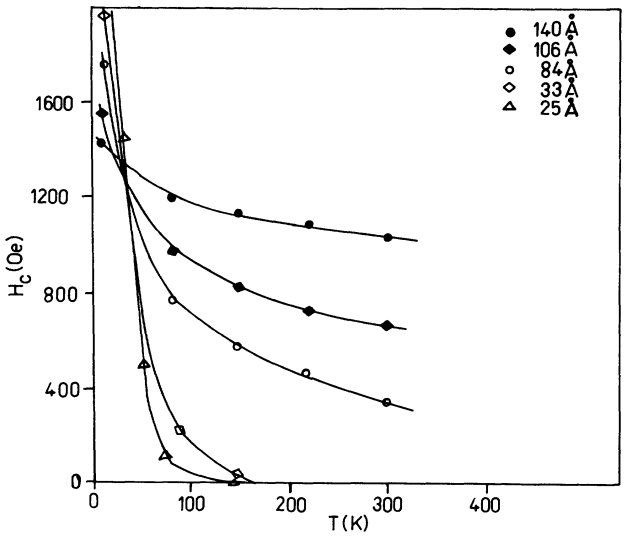

FIG. 14. Variation of coercivity with temperature for samples with median core diameter of 106, 84, 33, and 25 Å.

This increase in H_c might be related to the larger surface to volume ratio in the smaller particles. This could result in a higher effective anisotropy with large contributions, from the surface and interface anisotropy.

The coercivity of the fine Fe particles could not be explained by assuming the average values of magnetization and magnetocrystalline anisotropy for α-Fe and γ-Fe_2O_3/Fe_3O_4 and using the Stoner and Wohlfarth[31] model for noninteracting single domain particles with shape or magnetocrystalline anisotropy. The particles behave as if they are more anisotropic. Attempts were made to calculate the value of the effective anisotropy constant K from the magnetization data, using the law of approach to saturation[32] (the reduced remanence of the fine particles was very close to 0.5 indicating a random distribution of uniaxial particles):

$$M=M_s(1-b/H^2-c/H^3)+\chi_f H \ , \tag{6}$$

where b is a function of M_s and K and is equal to $\frac{4}{15}K_1^2/M_s^2$ for uniaxial polycrystalline structures, M_s is the saturation magnetization, and χ_f is the high-field susceptibility. Furthermore, the H_c vs $T^{1/2}$ law[33] was also used to find "K" graphically using the following expression:

$$H_c=2K/M_s-(2/M_s)(25k_BK/V)^{1/2}T^{1/2} \ , \tag{7}$$

where V is the median particle volume.

Both techniques gave values of K of the order of 10^6 erg/cm^3. Thus the experimental value of K is larger by an order of magnitude than the bulk Fe and Fe-oxide values. Similar values of K have also been reported by Xiao and Chien[24] in Fe-SiO_2 granular solids. The origin of such large effective anisotropy could be partly due to the shell-type particle morphology where the oxide coating is believed to interact strongly with the Fe core and partly due to the large surface effects which are expected in ultrafine particles.

The coercivity values obtained using the Stoner-Wohlfarth model and the values of effective K obtained from the law of approach to saturation [Eq. (8)], are listed in Table IV. The values of calculated coercivity for the larger particles were found to be of the same order as those measured experimentally. However, in the smaller spherical particles (where the shape effects are negligible), the deviations were much higher. The large differences cannot be explained only by the particle interactions. The dipole-dipole particle interactions would depend strongly on the magnetization values. Also the lower H_c values could not be explained by an incoherent rotation of magnetization process since the only incoherent mechanism which is size dependent is curling and this is a higher coercivity mechanism for particles with a size

TABLE IV. Coercivity values obtained with use of Stoner's Wohlfarth model and value of the effective K obtained from the law of approach to saturation.

Particle size d_{core} (Å)	K_1 (ergs/cm^3) [Eq. (6)]	H_c^K (Oe) uniaxial $\left[\frac{0.96K}{M_s}\right]$	H_c^K (Oe) cubic $\left[\frac{0.64K}{M_s}\right]$	H_c (Oe) Experimental ($T=10$ K)	M_s (expt.) (emu/g)
33	4.9×10^6	11 615	7600	2400	52.6
44	3.7×10^6	12 400	8098	2570	37.2
84	2.5×10^6	3 414	2230	1750	91.3
121	2.1×10^6	1 370	1000	1425	191

below single domain.

The results of these studies suggest that the coercivity of the particles is strongly influenced by the core-shell particle morphology and especially by the interaction between the Fe-oxide shell and the Fe core. This interaction is strongly reflected in the temperature dependence of coercivity as shown in Fig. 14. The highest H_c obtained at room temperature was 1050 Oe for a particle with a 140 Å core diameter, and its value at 10 K was 1425 Oe (only 37% higher), whereas, in a sample with a core diameter 25 Å the coercivity decreased from a value of 3400 Oe at 10 K to a negligible value at 150 K. Thus, in the smaller particles the temperature dependence of the coercivity is much stronger than in the bigger particles. In smaller particles the Fe core feels much more the effect of the Fe-oxide shell (due to higher Fe oxide to Fe ratio) and the absolute temperature coercivity due to exchange interaction at the core-shell interface is higher. Also the effect of surface anisotropy, if present, would be higher in the smaller particles. The strong decrease of coercivity with temperature can be explained from the superparamagnetic behavior of the Fe-oxide shell. The blocking temperature of the oxide shell as determined from Mössbauer analysis is approximately 300 K, which implies the onset of superparamagnetism at about 30 K when measured with a SQUID magnetometer. The crossover in the coercivity versus temperature curve (Fig. 14) also occurs at the same temperature. The effect of this superparamagnetic shell is to decrease the coercivity of the particle as the temperature increases (above 30 K), through exchange interaction at the core-shell interface.

This core-shell morphology and interfacial interaction has been considered by Trohidou *et al.*,[34] who predicted a modified H_c vs $T^{1/2}$ dependence [Eq. (7)] by taking into account the anisotropies of the Fe core, the Fe-oxide shell, the interface anisotropy, and the surface anisotropy. The model explained quite satisfactorily the experimental $H_c(T)$ data (Fig. 14) by considering one atomic layer thick interface with an effective anisotropy about ten times as large as that of the bulk Fe and a shell thickness of about 13 Å. This model could be further improved by taking into account the interparticle interactions.

IV. CONCLUSIONS

The magnetic, Mössbauer, and transmission electron microscopy data are all consistent, indicating a core-shell type of structure with a core consisting of α-Fe and a coating consisting of Fe oxides about 10–20 Å in thickness. The oxide layer is not continuous but consists of very fine grains. The interaction between the superparamagnetic shell and magnetically hard Fe core is responsible for the high coercivity values observed at low temperature and its drastic temperature dependence. The effect is more pronounced in smaller particles where the core is relatively small and fluctuations of the magnetic moment of the shell are large enough to make the whole particle magnetically soft.

ACKNOWLEDGMENT

This work has been supported by NSF-CHE-9013930.

*Also at Department of Chemistry
†Also at Institute of Material Science, NCSR Demokritos, Athens, Greece.

[1]E. Matijevic, Mater. Res. Bull. **XIV**, 19 (1989).
[2]M. Ozaki, Mater. Res. Bull. **XIV**, 35 (1989).
[3]A. Tasaki, S. Tomiyana, and S. Iida, Jpn. J. Appl. Phys. **4**, 707 (1965).
[4]A. Hayashi, J. Vac. Sci. Technol. A **5**, 1375 (1987).
[5]C. G. Granqvist and R. A. Buhrman, J. Appl. Phys. **47**, 2200 (1976).
[6]A. Tasaki, M. Oda, S. Kashu, and C. Hayashi, IEEE Trans. Magn. **MAG-15**, 1540 (1979).
[7]A. Tasaki, M. Takao, and H. Tokunaga, Jpn. J. Appl. Phys. **13**, 271 (1974).
[8]A. Tasaki, N. Saegusa, and M. Oda, IEEE Trans. Magn. **MAG-19**, 1731 (1983).
[9]A. E. Berkowitz, W. J. Schuele, and P. J. Flanders, J. Appl. Phys. **39**, 1261 (1968).
[10]A. H. Morrish, K. Haneda, and P. J. Schurer, J. Phys. (Paris) Colloq. **37**, C6-301 (1976).
[11]J. M. D. Coey and D. Khalafella, Phys. Status Solidi A **11**, 229 (1976).
[12]K. Haneda and A. H. Morrish, Surf. Sci. **77**, 584 (1978).
[13]You-Wei Du *et al.*, J. Appl. Phys. **61**, 3314 (1987).
[14]A. H. Pfund, Phys. Rev. **35**, 1434 (1930); J. Opt. Soc. Am. **23**, 375 (1933).
[15]H. C. Burger and P. H. van Cittert, Z. Phys. **66**, 210 (1930).
[16]L. Harris, R. T. McGinnies, and B. M. Siegel, J. Opt. Soc. Am. **38**, 582 (1948); L. Harris, D. Jefferies, and B. M. Siegel, J. Appl. Phys. **19**, 791 (1948).
[17]V. Papaefthymiou, A. Kostikas, A. Simopoulos, D. Niarchos, S. Gangopadhyay, G. C. Hadjipanayis, K. J. Klabunde, and C. M. Sorensen, J. Appl. Phys. **67**, 4487 (1990).
[18]H. Yamada, M. Takano, M. Kiyama, J. Takada, T. Shinjo, and K. Watanabe, Adv. Ceram. **16**, 169 (1985).
[19]O. Kubo, T. Ido, H. Yokoyama, and Y. Koike, J. Appl. Phys. **57**, 4280 (1985).
[20]F. E. Luborsky, J. Appl. Phys. **29**, 309 (1958).
[21]K. Haneda and A. H. Morrish, IEEE Trans. Magn. **25**, 2597 (1989).
[22]I. Tamura and M. Hayashi, Surf. Sci. **146**, 501 (1984).
[23]T. Shinjo, T. Shigematsu, N. Hosaito, T. Iwasaki, and T. Takai, J. J. Appl. Phys. **21**, L220 (1982).
[24]C. Kittel, *Introduction to Solid State Physics*, 5th ed. (Wiley, New York, 1976), p. 465.
[25]G. Xiao and C. L. Chien, J. Appl. Phys. **51**, 1280 (1987).
[26]D. L. Mills, Commun. Solid State Phys. **4**, 28 (1971).
[27]K. Haneda and A. H. Morrish, Nature **282**, 186 (1979).
[28]L. Néel, Ann. Geophys. **5**, 99 (1949).
[29]S. Mørup and H. Topsøe, Appl. Phys. **11**, 63 (1976).
[30]E. F. Kneller and F. E. Luberosky, J. Appl. Phys. **34**, 656 (1963).

[31]E. C. Stoner and E. P. Wohlfarth, Philos. Trans. R. Soc. London, Ser. A **240**, 599 (1948).
[32]B. D. Cullity, *Introduction to Magnetic Materials* (Addison-Wesley, Reading, MA, 1972), p. 347.
[33]B. D. Cullity, *Introduction to Magnetic Materials* (Ref. 32), p. 415.
[34]K. N. Trohidou, C. M. Soukoulis, A. Kostikas, and G. C. Hadjipanayis, in *Proceedings of the International Conference on Magnetism, Edinburgh, 1991,* edited by S. B. Palmer (to be published).

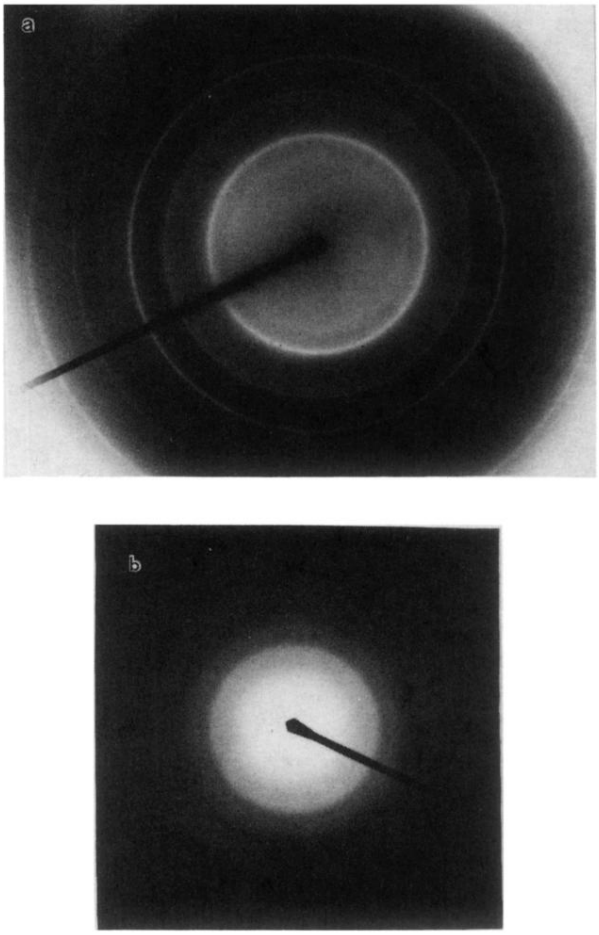

FIG. 1. (a) SAD of a sample with total diameter of 200 Å, showing sharp diffraction lines; (b) selected area diffraction pattern of a sample with total diameter of 68 Å, showing broad and diffuse lines.

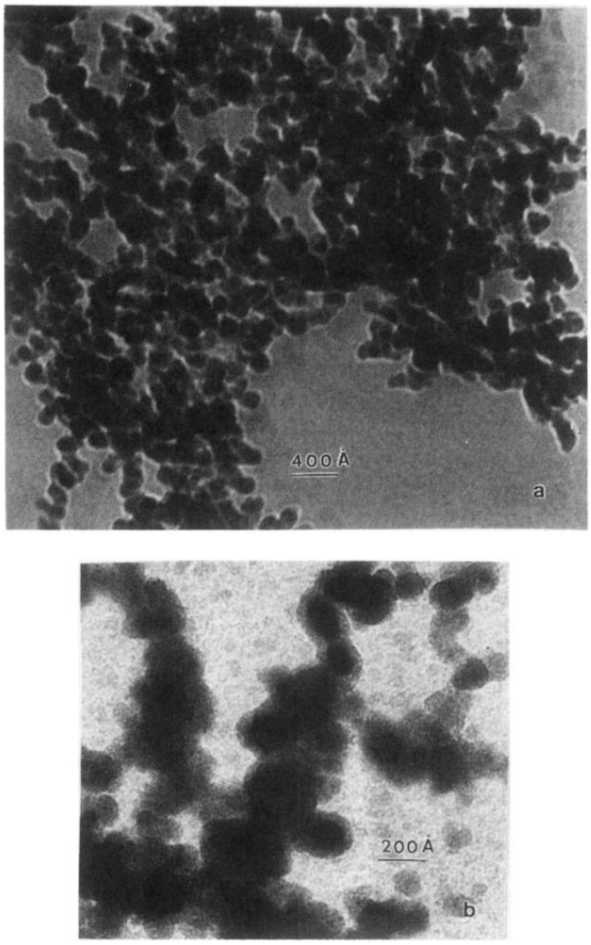

FIG. 2. (a) Bright-field micrograph showing nearly spherical particles of an Fe sample with median diameter of 110 Å; (b) bright-field TEM showing particles with clear dark centers surrounded by a light colored shell around them.